LCLS-II Technical Note

Resonant Excitation of High Order Modes in Superconducting RF Cavities of LCLS II Linac

LCLS-II TN- ~~14-XX~~ 15-06

3/2/15

Alexander Sukhanov, Alexander Vostrikov, Timergali Khabiboulline, Andrei Lunin, Nikolay Solyak, Vyacheslav Yakovlev

Resonant excitation of high order modes in superconducting RF cavities of LCLS II linac

Alexander Sukhanov, Alexander Vostrikov, Timergali Khabiboulline,
Andrei Lunin, Nikolay Solyak, Vyacheslav Yakovlev
Fermilab, Batavia IL 60510, US

Abstract

Estimation of losses caused by non-propagating and propagating longitudinal high order modes in superconducting linac of LCLS II is given.

Contents

1   Introduction

Design of the Linac Coherent Light Source II (LCLS II) at SLAC is currently underway [1]. When completed LCLS II will provide soft coherent X-ray radiation for a broad spectrum of basic research applications.

Since LCLS II is requited to operate in continuos wave (CW) regime, superconducting RF (SRF) technology has been chosen in order to minimize power consumption and operational cost of the facility. Main accelerating elements of LCLS II linac are TESLA-style 1.3 GHz 9-cell elliptical cavities, which are grouped in cryomodules (CM) of XEFL-type [2] modified for CW operation. Each cryomodule contains 8 cavities Layout of the LCLS II linac is shown in Fig. 1.

2   Monopole HOMs

CW bunched beam passing through SRF cavity may coherently excite HOMs with a high loaded quality factor, Q_L. If HOM is excited close to its resonance frequency, the effect may be significantly higher compared to incoherent losses. Also, in periodic structure of multiple SRF cavities in linac conditions may be realized when HOMs with frequency above beam pipe cut-off frequencyare effectively trapped inside cavities [3].

We have developed a model for estimation of resonance excitation of the HOMs and applied this model for the Project X CW SRF linac design [4, 5, 9, 10].
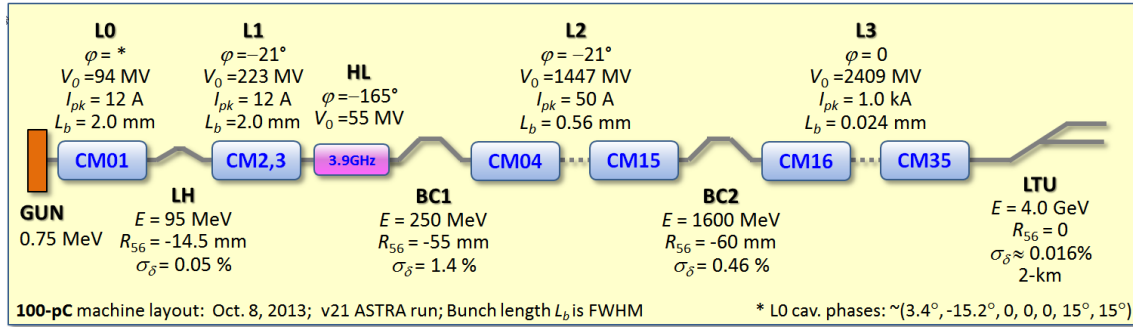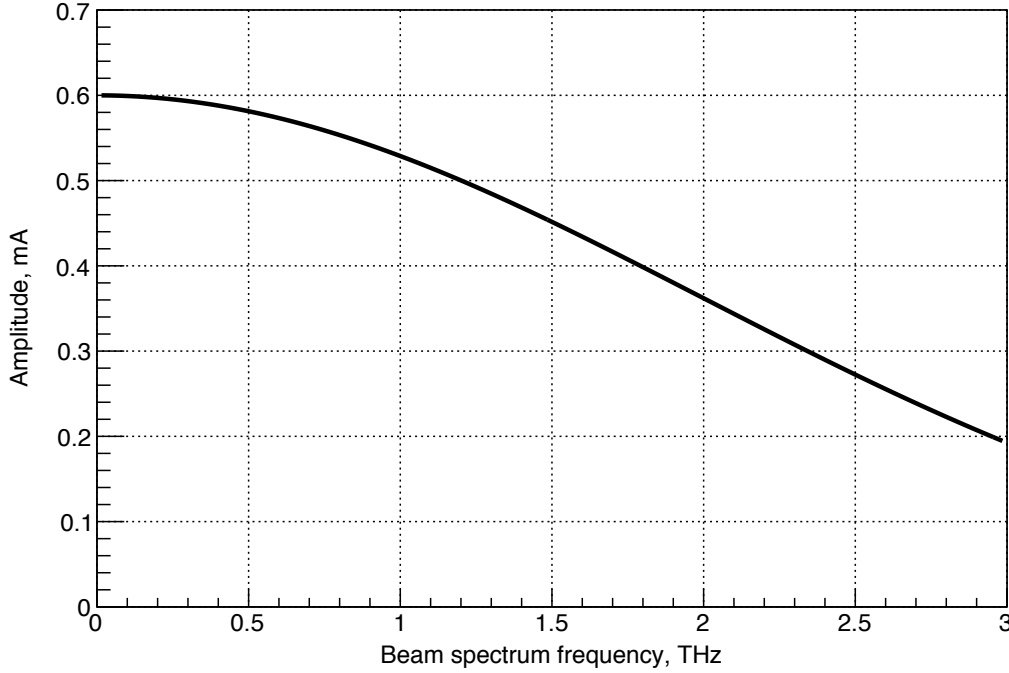
Figure 1: Schematic layout of LCLS II linac.

Figure 2: Beam spectrum for LCLS II in assumption of average current of 0.3 mA, bunch size of 80 fs ($L_b = 24\,\mu$m) and uniform particles distribution within bunches.

The basic features of our model in application to the analysis of HOMs in LCLS II linac are the following. We use a conservative approach and estimate the maximum possible effect. Since LCLS II bunch timing structure is very uniform, no significant effects on longitudinal beam dynamics are expected. Tesla-type 9-cell structure with HOM couplers and absorbers providing $Q_L < 10^6$ is assumed. We use SuperLANS RF simulation code [11] to calculate cavity spectrum. The worst trapping conditions for the propagating HOMs, when the (R/Q) values are at their maximum, are found by the variation of the distance between cavities in our model. Random variations of HOM frequencies from cavity to cavity with R.M.S. value $\sigma_f \sim 1$ MHz are assumed [12]. An idealized beam current spectrum without time and charge jitter is calculated.

2.1 Beam Spectrum

The bunch repetition frequency in LCLS II is assumed to be constant and equal to 1 MHz, and the bunch length is $\delta t_b = 80$ fs ($L_b = 24\,\mu$m). We suppose that bunches have the uniform charge distribution with the total charge $q_b = 0.3$ nC.

Calculated beam spectrum is shown in Fig. 2. Spectrum lines are separated by 1 MHz. One can see, that for the frequencies below 200 MHz the beam spectrum is quite flat.
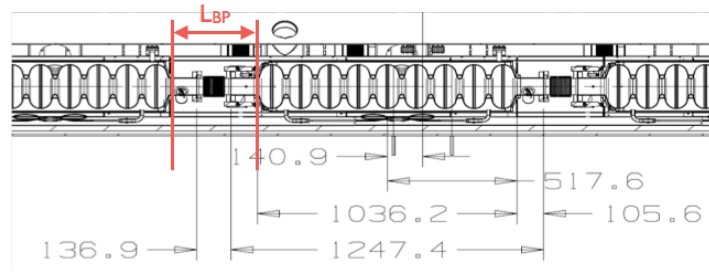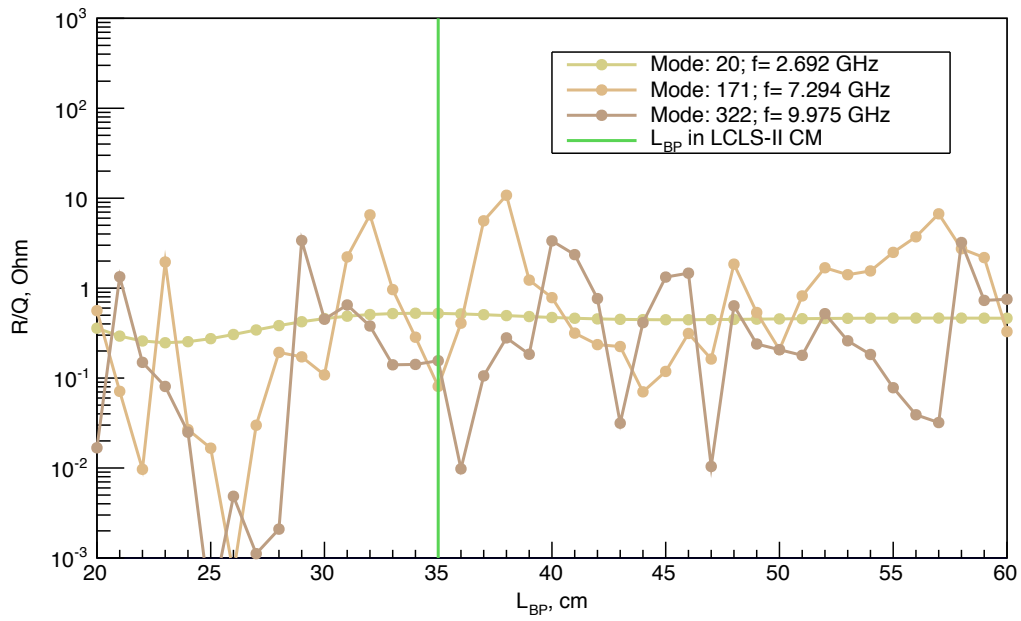
Figure 3: Layout of cryomodule.

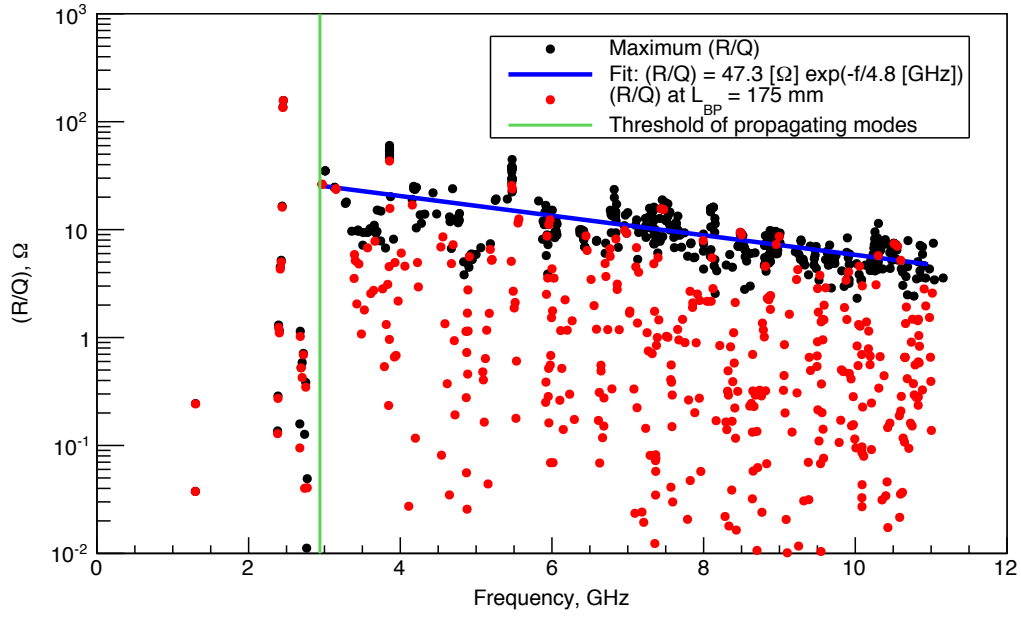Figure 4: (R/Q) *vs* beam pipe length.
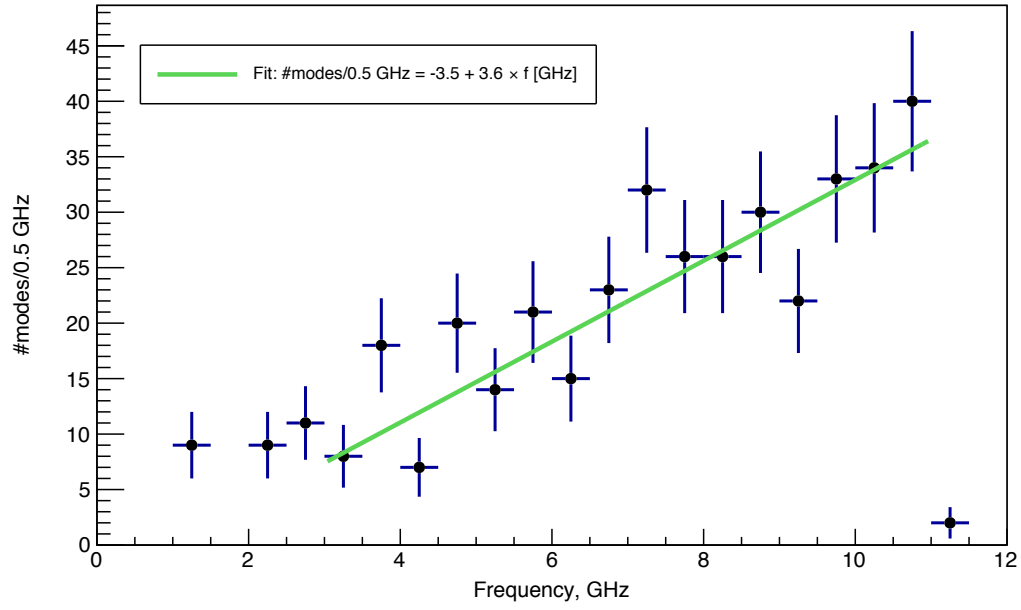
3

Figure 5: (R/Q) *vs* frequency.

Figure 6: Number of monopole HOM *vs* frequency.

2.2 HOM Spectrum

We evaluate HOM spectrum of Tesla-type 9-cell cavity using SuperLANS code. HOMs can be characterized as trapped or propagating by their relation to the beam pipe cut-off frequency. For longitudinal monopole modes the cut-off frequency in a cylindrical pipe is defined as $f_{\text{cutoff}} = 2\pi c \frac{\chi_{01}}{r} \approx 2\pi c \frac{2.4048}{r}$, where χ_{01} is the first root of $J_0(r)$ — the Bessel function of the first kind of order 0. For Tesla-type 9-cell 1.3 GHz cavity $f_{\text{cutoff}} = 2.94$ GHz.

Frequency of the trapped modes is below f_{cutoff}, while the propagating modes have frequency above the cut-off frequency.

Propagating modes can form standing waves in the structure of multiple cavities and became effectively trapped. Impedance (R/Q) of such trapped modes depend on where the standing wave is formed. In order to evaluate (R/Q) variations with the length of the standing wave in our simulation, we vary length of the beam pipe between cavities, $L_{\textbf{BP}}$, as shown in Fig. 3. As an example, Fig. 4 shows effective impedance (R/Q) of three different modes as a function of the distance between cavities (note, that the green line shows nominal distance in LCLS II cryomodule). Mode 20 in this plot has frequency $f_{20} = 2.692$ GHz which is below the cut-off frequency and thus is not sensitive to the variations of the beam pipe. Modes 171 and 322 with frequencies $f_{171} = 7.294$ GHz and $f_{322} = 9.975$ GHz are above the cut-off frequency. Both of these modes display large variations in (R/Q) from a fraction of mΩ to about 10 Ω. Most favorable trapping conditions happen when (R/Q) value is at its largest.

Spectrum of the monopole HOMs of Tesla-type 9-cell cavity is shown in Fig. 5. In this plot black dots show the maximum value of (R/Q) while $L_{\textbf{BP}}$ changes from 20 to 60 cm. Red dots correspond to the values of (R/Q) at the nominal LCLS II beam pipe length ($\sim$35 cm). We approximate dependence of the impedance on the mode frequency by an exponential function $(R/Q)[\Omega] = 47.3 \exp(-f/4.8[\text{GHz}])$. It is interesting to note, that the density of the monopole modes increases approximately linearly with the frequency, with the slope parameter ~ 3.6 modes/(GHz)^2, as shown in Fig. 6.

2.3 Power Loss Calculation

For each mode we calculate losses in cavity walls and bellows and the corresponding quality factors, Q_0 and Q_b.

Surface resistance of superconducting Nb, according to [6] is

$$R_s = R_{res} + R_{BCS}\,, \tag{1}$$

where $R_{res} = 1$ nΩ, and BSC part is parameterized as

$$R_{BSC}[\Omega] = \frac{2 \cdot 10^{-4}}{T[\text{K}]} \left(\frac{f[\text{GHz}]}{1.5} \right)^2 \exp\left\{ -\frac{17.67}{T[\text{K}]} \right\}\,. \tag{2}$$

We use simplified geometry of bellows with the following assumptions. The bellow is modelled as a cylinder with the beam pipe radius. Surface field variations are small at the length of the single bellow convolution. Take into account larger bellow surface by multiplying results by a factor of 2–3 (depends on specific geometry of bellow). For stainless steel bellow we assume normal skin effect with SS conductivity $\sigma_{SS} = 2$ MSi, and $R_s \sim \omega^{1/2}$. There is anomalous skin effect in copper at 4.5 K in GHz frequency range, therefore for copper plated bellows we use $R_s = A\omega^{2/3}$, where $A = 3.3 \cdot 10^{-10} \Omega \text{s}^{2/3}$ [7, 8]. Figure 7 shows calculated Q-factors.

HOM power is partially removed through HOM couplers and power coupler (Q_h). Measurements of Q_h for non-propagating modes at DESY (J. Sekutowicz) and Fermilab (T. Khabiboulline): $Q_h < 2 \cdot 10^5$. This value may vary due to small variations in cavity geometry because of manufacturing tolerances. Trapped modes may have higher value of Q_h. We use the following values in our analysis: $Q_h = 2 \cdot 10^5, 10^6, 10^7$.

Total power loss by HOMs is characterized by loaded Q-factor:

$$1/Q_L = 1/Q_0 + 1/Q_h + 1/Q_b\,. \tag{3}$$

Magnetic field on the surface of cavity induced by the nth component of the beam spectrum is equal to the sum of all exited modes:

$$H_n = \sum_p H_{pn}(z)\,, \tag{4}$$

where

$$H_{pn} = \frac{-i\omega_p^2}{\omega_n^2 - \omega_p^2 - i\frac{\omega_n \omega_p}{Q_p}} \frac{I_n}{2} \sqrt{\frac{(R/Q)_p}{\omega_p W_p}} H_p^{sim}(z)\,. \tag{5}$$

Here $H_p^{sim}(z)$ is the field calculated by RF simulation code for mode p, ω_p is the mode frequency, W_p is the mode stored energy normalized by LANS to 1 mJ, Q_p and $(R/Q)_p$ are the mode (loaded) quality factor and impedance, I_n and ω_n are the amplitude and frequency of beam harmonic. Total power loss in the cavity walls is calculated as sum of losses by individual beam harmonics. Expression for $|H_n|^2$ contains cross-terms $H_{pn} H_{qn}^*$ which have extremely small contribution and can be neglected. Total power loss is

$$P_{(0,h,b)} = \sum_p \sum_n \frac{\omega_p^4}{(\omega_n^2 - \omega_p^2)^2 + \left(\frac{\omega_n \omega_p}{Q_p} \right)^2} \frac{I_n^2}{4} \left(\frac{R}{Q} \right) \frac{1}{Q_{(0,h,b)}}\,. \tag{6}$$
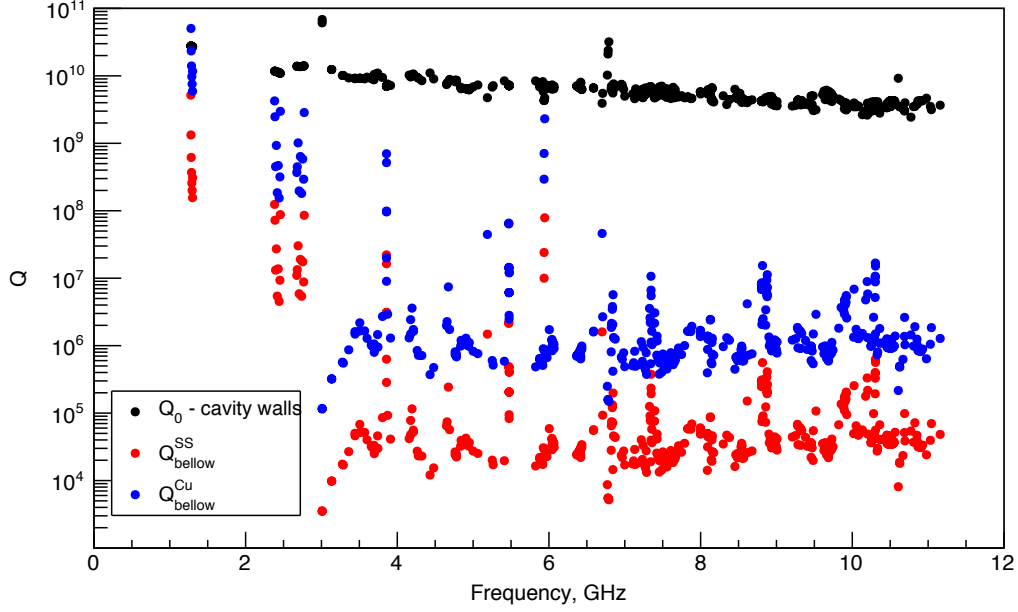
Figure 7: HOM quality factors corresponding to the losses in the cavity walls (black dots) and in the bellows (red dosts for stainless steel and blue for copper coated) *vs* frequency.

2.4   Results

We simulate 10^5 cavities with random variations of the HOM frequency with R.M.S. value $\sigma_f = 1$ MHz. In order to obtain conservative estimation we use maximum value of the effective impedance (R/Q), as described in Sec. 2.2. Results are presented as *complimentary cumulative distribution function* $(CCDF)$[1] of power loss.

2.4.1   Losses in cavity walls

Distribution of power loss in the cavity walls is shown in Fig. 8. In this plot contributions from non-propagating modes with frequencies $f < 2.9$ GHz are shown by black, red and green lines for $Q_h = 2 \cdot 10^5$, 10^6 and 10^7, respectively. Blue ($Q_h = 10^6$) and cyan ($Q_h = 10^7$) lines show distributions for all HOM with frequencies up to 10 GHz.

The median power loss, which corresponds to probability of 0.5, is approximately 1 μW for non-propagating modes. When all HOM up to 10 GHz are included, median power loss increases up to 1 mW.

Occasionally, due to random variation of its frequency, a single HOM in one cavity may come close to resonance. In this case power loss may increase up to 100 mW, although probability of such event is extremely low, it is less than 10^{-3}.

We conclude, that cryogenic losses due to resonace excitation of monopole HOM are small.

2.4.2   Power removed by HOM couplers

Figure 9 shows distribution of power removed by HOM couplers. Note that this power is calculated for two couplers combined (also some power is removed by main coupler) and power flow through one HOM coupler is at least twice lower. Black line in this plot corresponds to $Q_h = 10^5$. Results for $Q_h = 10^6$ are shown by solid red line. Median power is approximately 20 mW. When one of the HOM is close to resonance, power flow though HOM couplers may be as high as approximately 10 W, but probability of this to happen is about 10^{-3}.

In Fig. 9 we also demonstrate effect of HOM frequency manipulation. The idea behind this is that when the main accelerating mode of the cavity is detuned and then tuned back to nominal value (1.3 GHz), the spectrum of HOM is shifted due to plastic deformations of the cavity. Dashed, dotted-dashed and double dotted-dashed lines in Fig. 9 show results of frequency shifts by 100, 300 and 1000 Hz, respectively. As expected, shift of HOM frequency by 1000 Hz (which approximately corresponds to the width of the resonance with $Q_h = 10^6$) is enough to reduce power flow in HOM couplers to about 8 W (less than 4 W per coupler) with the probability 10^{-4}.

We conclude that power removed by HOM couplers for majority of the cavities (99%) is less than 1 W. In a rare case when in one cavity one of the HOM is close to resonance frequency manipulation procedure can be used in order to move HOM away from resonance.
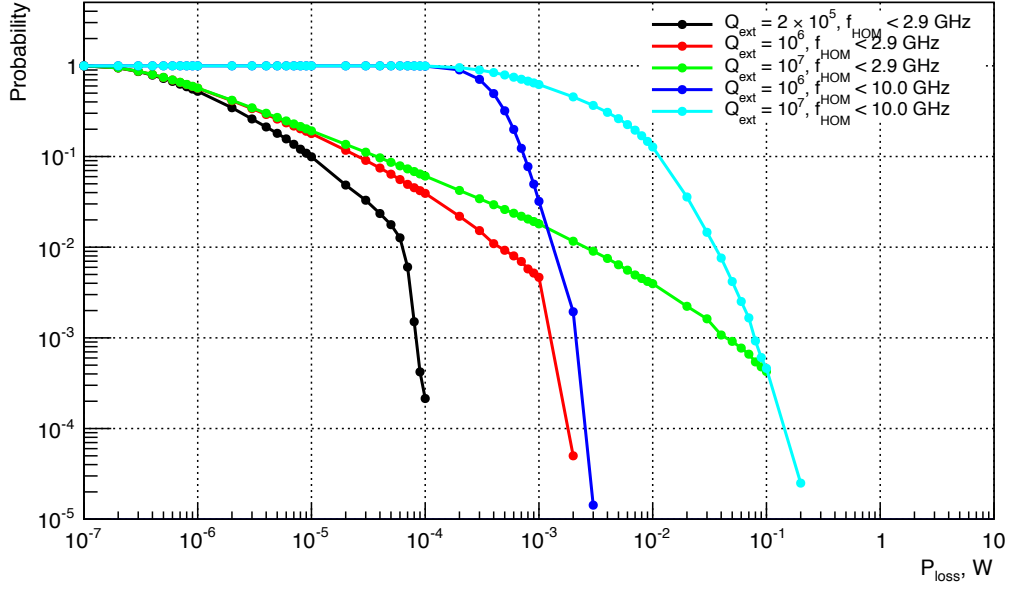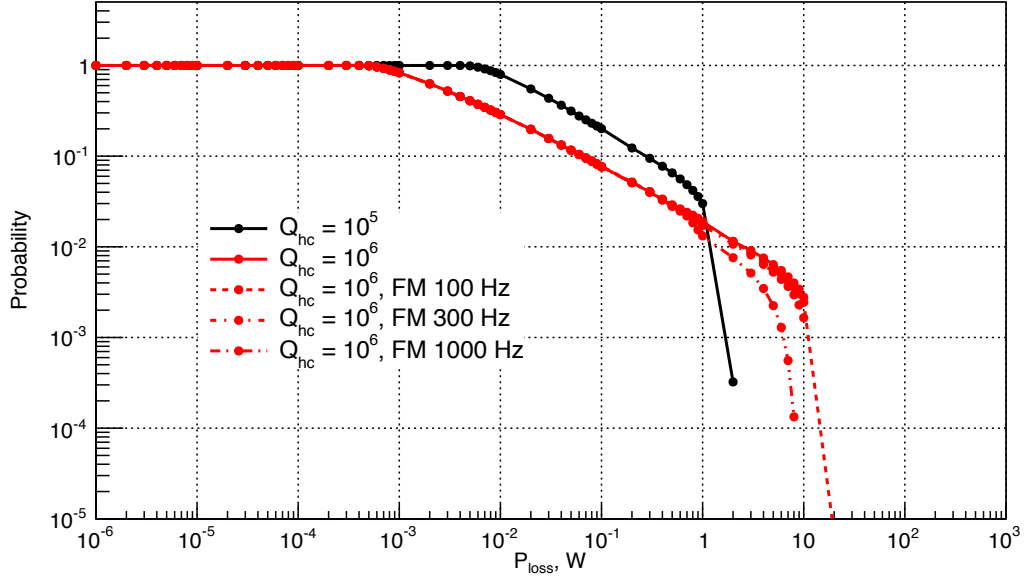
Figure 8: Power dissipation in cavity walls.

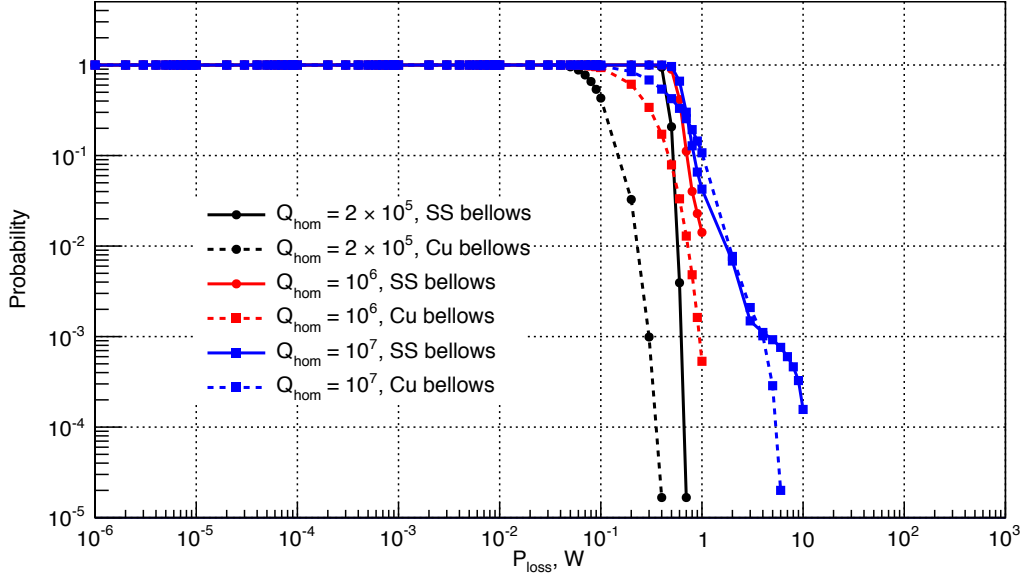Figure 9: Power removed by HOM couplers.

7

Figure 10: Power dissipated in bellows.

2.4.3 Power dissipation in bellows

Figure 10 shows distribution of losses in bellows. Black, red and blue lines correspond to $Q_h = 2 \cdot 10^5$, Q^6 and Q^7, respectively. Results for stainless steel bellow are shown by solid lines, for copper plated bellows — by dashed lines. As one may expect more power is dissipated in the stainless steel bellows, with the median loss about 0.6 W. If we exclude extreme cases with very inefficient HOM couplers ($Q_h = 10^7$), and consider only copper plated bellows, we find that median power dissipation can reach 1 W with probability less than 10^{-3}.

We conclude that resonance HOM excitation should not be a problem for copper plated bellows, if $Q_h \leq 10^6$.

2.5 Transition effects on the longitudinal beam dynamics

In LCLS-II beam bunches are deflected to different undulators or to beam diagnostics section. It may results in periodic shifts of bunches between adjacent RF buckets of accelerating mode. If a monopole HOM is already excited in cavity by previos bunches, the shifted bunches see this mode in "wrong" phase. During the transition, while HOM is catching up with the new phase of bunches, bunch energy may vary, depending on the initial phase difference. The largest transition effect is when the phase difference is 180 degree. This can be estimated as the following:

$$\Delta V = \frac{1}{2} \left(\frac{R}{Q} \right) Q_L I = 1.5 \, \text{kV} , \qquad (7)$$

where we assumed $(R/Q) = 10\,\Omega$, $Q_L = 10^6$ and beam current $I = 0.3$ mA. Since phase shift is random from mode to mode and from cavity to cavity we may assume that the maximum average effect on the bunch energy variations during transition do not exceed $\langle \Delta V \rangle = 1/2 \Delta V = 0.75$ kV.

We conclude, that variations in bunch energy during transitions due to changes in bunch timing structure, should not be a problem if $Q_L \leq 10^6$.

3 Very High Frequency HOMs

Due to the very short longitudinal bunch size, the LCLS II beam current spectrum extends into THz range. This means, that some sizable fraction of EM energy radiated by bunches is in the frequency region above the energy gap of Cooper pairs in superconducting niobium, which corresponds to 750 GHz at 2 K. Absorption of EM radiation above this frequency in niobium breaks Cooper pairs and increases normal conducting phase, resulting in the increased surface resistance and deterioration of the cavity intrinsic quality factor, Q_0.

In order to estimate losses into very high frequency modes, we use a diffraction model, following P. Hülsmann *et. al* [13]. According to this model, energy lost in a pill-box cavity of length L_{cell} by a bunch of longitudinal size σ_z and charge q_b coming from a beam pipe of radius a is

$$\Delta E_{1cell} = \frac{q_b^2}{4\pi\epsilon_0 a} \sqrt{\frac{L_{cell}}{2\sigma_z}} , \qquad (8)$$

---

[1]This is also called *tail distribution* or *exceedance* in literature. $CCDF(x)$ is the probability $P(X > x)$ to find random variable X to be greater that certain value x.
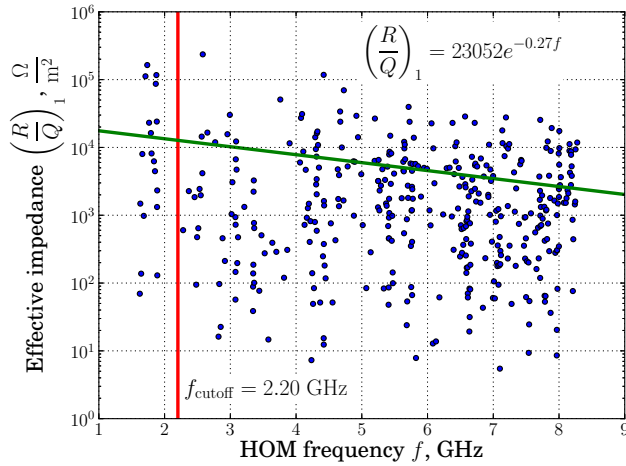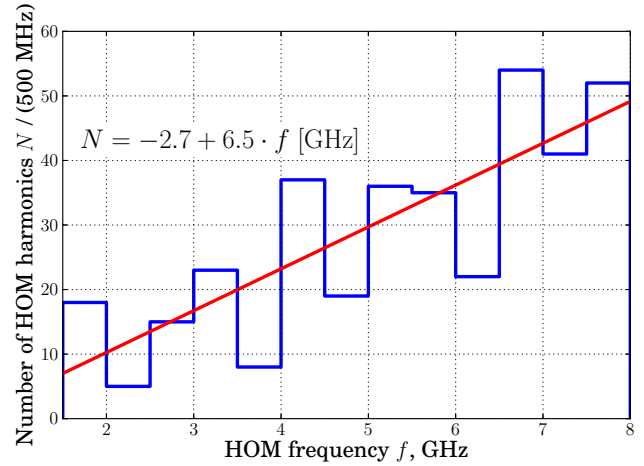
Figure 11: Dipole HOM spectrum.

Figure 12: Dipole HOM spectrum density.

where ϵ_0 is permittivity of free space. For LCLS II the largest effect is achieved when $q_b = 0.3$ nC, $\sigma_z = 50$ μm. For these parameters $\Delta E_{1cell} \approx 0.7$ μJ. As bunches travel through consecutive cells in multi-cavity structures (cryomodules) the losses per cell become smaller, as the energy density of the bunch EM field in the cell iris radius decreases due diffraction in previous cells. It has been shown in [13], that after about 200 cells energy lost per 9-cell structure $\Delta E_{9cell} \approx \Delta E_{1cell}$.

Average power loss is $P_{loss} = f_b \Delta E_{9cell} \approx 0.7$ W/cavity (here $f_b = 1MHz$ is bunch frequency). Only a fraction r of this losses is radiated in the frequency region above 750 GHz. We can estimate this fraction, assuming the following frequency dependence of the energy density of diffracted field: $\frac{dE}{d\omega} \sim \frac{e^{-\sigma_z^2 \omega^2 / c^2}}{\sqrt{\omega}}$. Then

$$ r = \int_{\omega_g}^{\infty} \frac{dE}{d\omega} d\omega \bigg/ \int_0^{\infty} \frac{dE}{d\omega} d\omega \approx 0.2 \,, \qquad (9) $$

where ω_g is circular frequency corresponding to 750 GHz. Thus, we expect that the average power loss above the energy gap of Cooper pairs in niobium is less than 0.2 W/cavity for LS beam parameters.

We conclude that power loss into very high frequency HOM should not be a problem in LCLS II CW linac.

4   Dipole HOMs and Cumulative Effects

A charged particle passing through a cavity can excite transverse dipole modes in it. It happens if the particle trajectory does not correspond with the cavity axis. Excitation of the dipole mode does not affect the particle motion, but the excited mode can interact with the following particles. That is why the effect is called cumulative. The following particles experience transverse kick due to interaction with the mode. This may result in effective emittance dilution over the time or even to beam break-up (BBU) effect. The significance of cumulative HOM excitation effects for the LCLS-II linac is estimated in this section.

Due to necessity of beam diagnostic or deflection bunch structure can be disturbed. It results in periodic sudden HOM phase shift, which causes the electron bunch transverse coordinate variation. Significance of the transverse coordinate variation is estimated. HOM phase shift frequency is discussed.

4.1   Dipole HOM spectrum

Dipole HOM spectrum is calculated using CLANS code, module "clans2". The code calculates HOM frequencies and effective impedances $R^{(1)}/Q$.

All HOMs can be characterized as trapped or propagating. Trapped HOM field is located within one cavity, while propagating modes transfer energy along the linac. Frequency of trapped modes is less than cut-off frequency. Propagating modes have frequency greater than cut-off frequency. For transverse dipole HOM in a circular cavity of radius r cut-off frequency defined as:

$$ f_{\text{cutoff}} = 2\pi c \frac{\chi_{11}}{r} \approx 2\pi c \frac{1.8412}{r}, \qquad (10) $$

where χ_{11} is the first root of $J_1(r)$ — the Bessel function of the first kind of order 1, and c is the speed of light.

In spite of propagating modes are not trapped inside one cavity, they might form a standing wave in the system with multiple cavities. In this case they produce the same effect as the trapped ones. That is why both propagating and trapped HOMs are considered in analysis. $R^{(1)}/Q$ of propagating modes depends on where the standing wave formed.
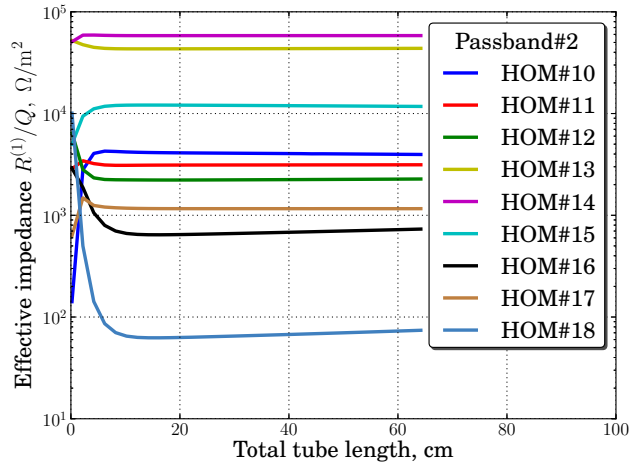
Figure 13: Dipole HOM effective impedance as a function of tube length for the second passband.
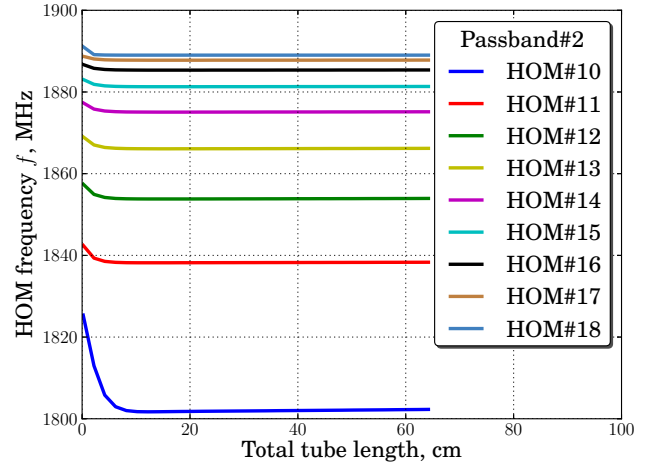

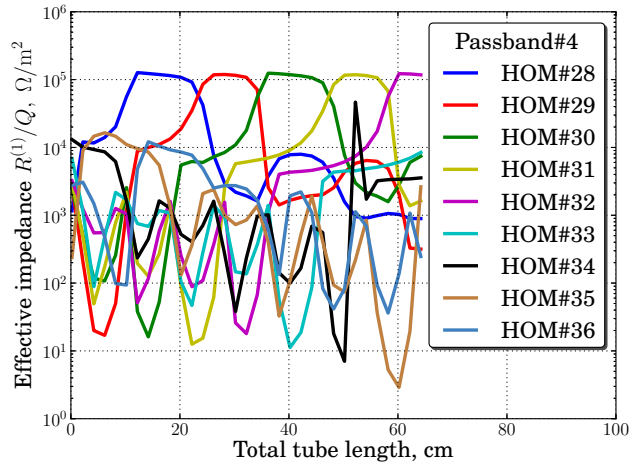Figure 14: Dipole HOM frequency as a function of tube length for the second passband.

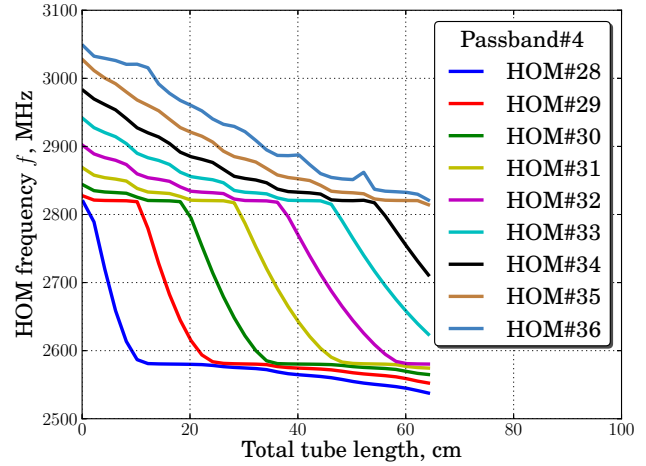Figure 15: Dipole HOM effective impedance as a function of tube length for the fourth passband.

Figure 16: Dipole HOM frequency as a function of tube length for the fourth passband.

Dipole HOM spectrum and spectrum density for 1.3 GHz ILC cavity are shown in Figures 11 and 12 correspondingly. Cut-off frequency for this type of cavity is 2.20 GHz. The spectrum density increases with HOM frequency (see Figure 12), but the effective impedance tends to decrease (see Figure 11). In the demonstrated case there is tube from both sides of the cavity. Total length of the tube is 29.6 cm. It defines the location of where propagating modes form. For this tube length HOM with the largest $R^{(1)}/Q$ is in fourth passband.

The dipole HOMs effective impedance as a function of total tube length is shown in Figure 13 for the second passband and in Figure 15 for the fourth one. Length of the tube from both sides of the cavity is the same. Passband #2 consists of trapped HOMs, thus effective impedance of the modes might vary when the total length of the tube is small, but it is constant when the tube is long enough. This behavior is explained by the fact that field of a trapped mode can go to the tube, but only for a short limited distance. Passband #4 consists of propagating modes. The effective impedance as a function of the tube length has maximums and minimums. Moreover, HOMs have maximum $R^{(1)}/Q$ value consequently. The upper limit on $R^{(1)}/Q$ for this passband can be defined from Figure 15. $R^{(1)}/Q$ of each HOM is always smaller than 275 kΩ/m^2. Note, that maximum value of effective impedance within the passband does not vary a lot with tube length. It allows to conclude that values of $R^{(1)}/Q$ in Figure 11 not much differ from the maximum possible effective impedance. Consequently, the limit of 275 kΩ/m^2 can be applied to all HOMs.

Dependence of HOMs frequency on the total tube length is shown in Figure 14 for the second passband and in Figure 16 for the fourth one. The plots demonstrate that HOM frequency of trapped modes does not depend on the tube length (when the tube is long enough), while the propagating modes change their frequency depending on the tube length significantly. The frequency may change up to 300 MHz within 30 cm tube length variation, which is much greater than the distance between two neighboring lines in the beam spectrum (1 MHz). Therefore, all positions of HOM frequency with respect to beam spectrum lines have to be considered.

Finally, separation between HOMs frequency is significant compare to the distance between two neighboring lines in the beam

spectrum. That is why each line of the beam spectrum interacts with one HOM only. Besides, when effective impedance of one HOM is in maximum, effective impedances of the rest of HOMs are much smaller. All these allows to consider a single HOM in the simulations. To get the upper limit on emittance dilution or beam transverse coordinate disturbance, the maximum value of $R^{(1)}/Q$ should be considered.

4.2 Model assumptions

The model for estimation of resonance excitation of HOMs, BBU effect and klystron-type instabilities has been developed. This model was applied for Project X CW SRF linac design [4].

The basic features of the model are the following. A conservative approach to estimate the maximum possible effect is used. TESLA-type 9-cell cavities with HOM couplers and absorbers providing loaded quality factor $Q_L < 10^7$ are assumed. SuperLANS RF simulation code is used to calculate HOM spectrum. Both trapped and propagating modes are calculated. $R^{(1)}/Q$ of a propagating mode depends on where it is trapped. The worst trapping conditions for propagating modes are assumed. The conditions are found by variation of the tube length, i.e. location of the mode (for example, see Figures 13 and 15). Two tube parts of the same length are attached to the cavity at each side for the $R^{(1)}/Q$ calculation. The maximum $R^{(1)}/Q$ value is used for the calculations. Dipole HOM spectrum is shown in Figure 11. The accelerator definition of the dipole mode impedance is used:

$$\frac{R^{(1)}}{Q} = \frac{\left| \int \left(\nabla_\perp E_z \right) \big|_{x=x_0} e^{i\omega z/v} \mathrm{d}z \right|^2}{\omega W_0}, \tag{11}$$

where E_z is HOM electric field along the axis of the cavity, v is beam velocity, ω is HOM circular frequency, and W_0 is HOM stored energy. The integral is taken along the line parallel to the cavity axis at the distance x_0. Random variation of HOM frequencies from cavity to cavity with RMS value of $\sigma_f = 1$ MHz is assumed if other is not specified. An idealized beam spectrum (Figure 2) is used without time and charge jitter. The charge of the bunches is 300 nC. The bunches follow with frequency of 1 MHz.

A bunch of charged particles passing through an SRF cavity excites dipole HOMs if displaced from the cavity axis. Excited HOMs with high quality factor store the energy long enough to affect the following bunches motion. Therefore each of the following bunches experience a transverse kick from HOM field and produce additional excitation of HOMs. As the result, the bunches change their angular components of motion, which causes effective transverse emittance dilution or may cause even beam break-up.

HOM voltage ΔU induced by a single bunch passing through a cavity can be calculated as

$$\Delta U = \frac{i}{2} c q_b \frac{R^{(1)}}{Q} (x - x^*), \tag{12}$$

where q_b is bunch charge, x is bunch position along x-axis, x^* is cavity misalignment along x-axis. When there are no bunches passing through the cavity, HOM voltage oscillates with time:

$$U(t) = U(0) e^{i\omega_m t - \frac{\omega_m t}{2Q}}, \tag{13}$$

where $\omega_m = 2\pi f_m$ is HOM circular frequency. Transverse kick on a bunch by HOM voltage U is

$$\Delta x' = \frac{e \mathrm{Re} U}{pc}. \tag{14}$$

HOM frequency itself does not affect the value of emittance dilution, but its difference with the closest beam spectrum line does. LCLS–II beam spectrum is regular (a line every 1 MHz), that is why distance from HOM to the closest beam spectrum line may vary from 0 (resonance case) to 500 kHz.

4.3 Emittance dilution

Simulation of the whole linac is performed to estimate BBU effect. Different HOM frequency spread from 1 Hz to 10 MHz is considered in this simulation. Note that actual HOM frequency spread is expected to be about 1 MHz, but the whole range of the spread is considered to demonstrate the dependence of the effect on the HOM frequency spread. For each value of the spread a set of linacs is simulated and effective transverse emittance dilution is calculated. Emittance dilution caused by HOM effects is taken into account. This emittance is compared to the designed bunch emittance. Relative effective transverse emittance is defined as a ratio of the actual effective transverse emittance to the design transverse emittance of the bunches.

Relative effective transverse emittance dilution due to a dipole HOM as a function of HOM frequency spread for two extreme cases (resonance and the farthest from the resonance) is shown in Figures 17 and 18 respectively. For the resonant case (Figure 17) emittance dilution goes to zero when HOM frequency spread goes to zero. This can be explained considering the extreme case when HOM frequency spread is zero. The first bunch passing through each cavity induces HOM voltage according to the Equation (12). HOM voltage oscillates according to the Equation (13) and as far as the case is resonant and HOM frequency spread is zero $\omega_m t = 2\pi n$, which means that when the next bunch is passing the cavity HOM frequency has imaginary value and does not provide any transverse kick to the bunch (see Equation (14)). Thus none of the bunches experience transverse motion disturbance due to HOM and emittance dilution is zero. The resonant case has a maximum of emittance dilution when frequency spread is equal to f_{HOM}/Q, which is 20 kHz for considered values. For the non-resonant case emittance dilution monotonic increase is explained by increase of probability for HOM frequency to be close
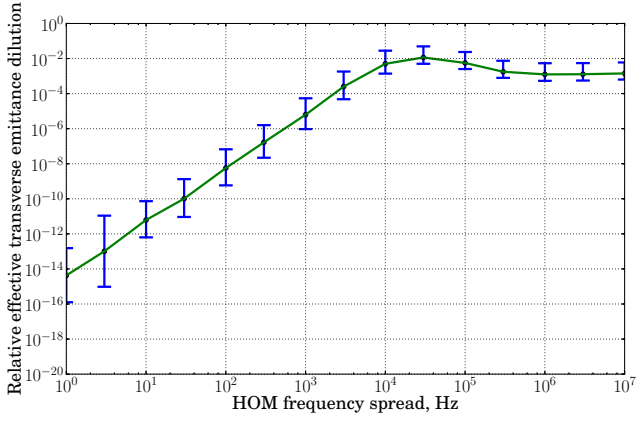
Figure 17: Relative effective transverse emittance dilution due to dipole HOM as a function of HOM frequency spread for the resonant case.
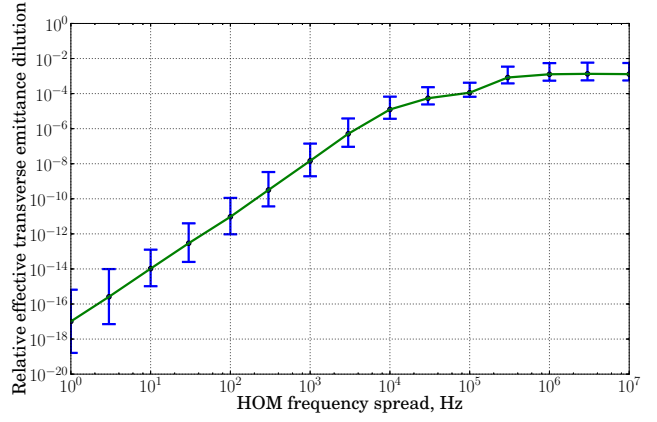
Figure 18: Relative effective transverse emittance dilution due to dipole HOM as a function of HOM frequency spread for the non-resonant case.

enough to the beam spectrum line. There is a significant jump in emittance dilution at about 0.5 MHz related to the distance between the central HOM frequency and closest beam spectrum line.

One can see that even for the worst case scenario effective transverse emittance dilution due to dipole HOM is less than 10% of the initial transverse emittance. This scenario is realized at HOM frequency spread of 20 kHz, which is far enough from the expected 1 MHz frequency spread. For actual value of HOM frequency spread expected relative emittance dilution is about 0.1%, which is negligible.

4.4 Transition effect

For electron beam deflection between two undulators in LCLS-II, the beam will shift to another RF bucket, thus RF deflector (operating at 325 MHz frequency) will shift the beam by 180 degrees (or 90 degrees if the beam will be sent to the dump line). Besides, single bunches periodically can be deflected for diagnostic purposes. In both cases beam phase suddenly changes. BBU transition effects due to sudden beam phase change is considered in this section.

Expected beam phase shift is 90 or 180 degrees of 325 MHz frequency (in case of shift to another RF bucket) and 360 degrees of 1 MHz frequency (in diagnostic case). As demonstrated in Section 4, HOM central frequency cannot be determined precisely (see Figure 16), that is why effective HOM phase shift can have different values. The most significant effect is observed when HOM phase shift is 180 degrees of HOM frequency. Various HOM phase shift frequency is considered to estimate allowed frequency of diagnostic bunch extraction.

In the situation when there is no transition effect and all bunches follow each other with constant time interval of 1 μs transverse coordinate of each bunch at the exit of the linac is presented in Figure 19a. There is some transverse coordinate variation (up to 80 mum) in the first bunches, but after 5 ms it goes to zero. When there is a sudden change of HOM phase by 180 degrees, real and imaginary parts of induced HOM voltage are swapped (see Equation (13)). Thus, each of the following bunches experience unexpected transverse kick which results in additional bunch transverse coordinate variation as demonstrated on Figure 19b. The variation from transition effect can be even greater than variation in the first bunches (130 μm compare to 80 μm for considered case).

The results of the simulation of periodic transition effect is shown in Figure 19c for 500 Hz HOM phase shift and in Figure 19d for 1 kHz HOM phase shift. One can see that when the frequency of HOM phase shift is small enough, there is not correlation between transition effects from each shift and beam transverse coordinate variation does not accumulate (Figure 19c). When the frequency increases, variations from the shifts accumulate (Figure 19c), but after few periods transverse coordinate oscillation comes to a steady regime when amplitude does not change anymore.

It is found that BBU transition effect results is up to 200 μm bunch center position disturbance when HOM phase shift frequency is below 1 kHz. This value satisfies the requirements for LCLS-II beam dynamics.

5 Conclusion

We estimated effects of resonance HOM excitation in LCLS II linac. We conclude, that cryogenic losses due to resonace excitation of monopole HOM are small. We conclude that power removed by HOM couplers for majority of the cavities (99%) is less than 1 W. In a rare case when in one cavity one of the HOM is close to resonance frequency manipulation procedure can be used in order to move HOM away from resonance. We conclude that resonance HOM excitation should not be a problem for copper plated bellows, if $Q_h \leq 10^6$. We conclude that power loss into very high frequency HOM should not be a problem in LCLS II CW linac.

Cumulative HOM excitation results in transverse emittance dilution. It is demonstrated that for expected HOM parameter (i.e. 1 MHz frequency spread) due to HOM transverse emittance increases by 0.1% of its initial value. It allows us to conclude that there is no need

(a) HOM phase shift is off.

(b) Sudden HOM phase shift by 180°.

(c) Periodic 500 Hz HOM phase shift by 180°.
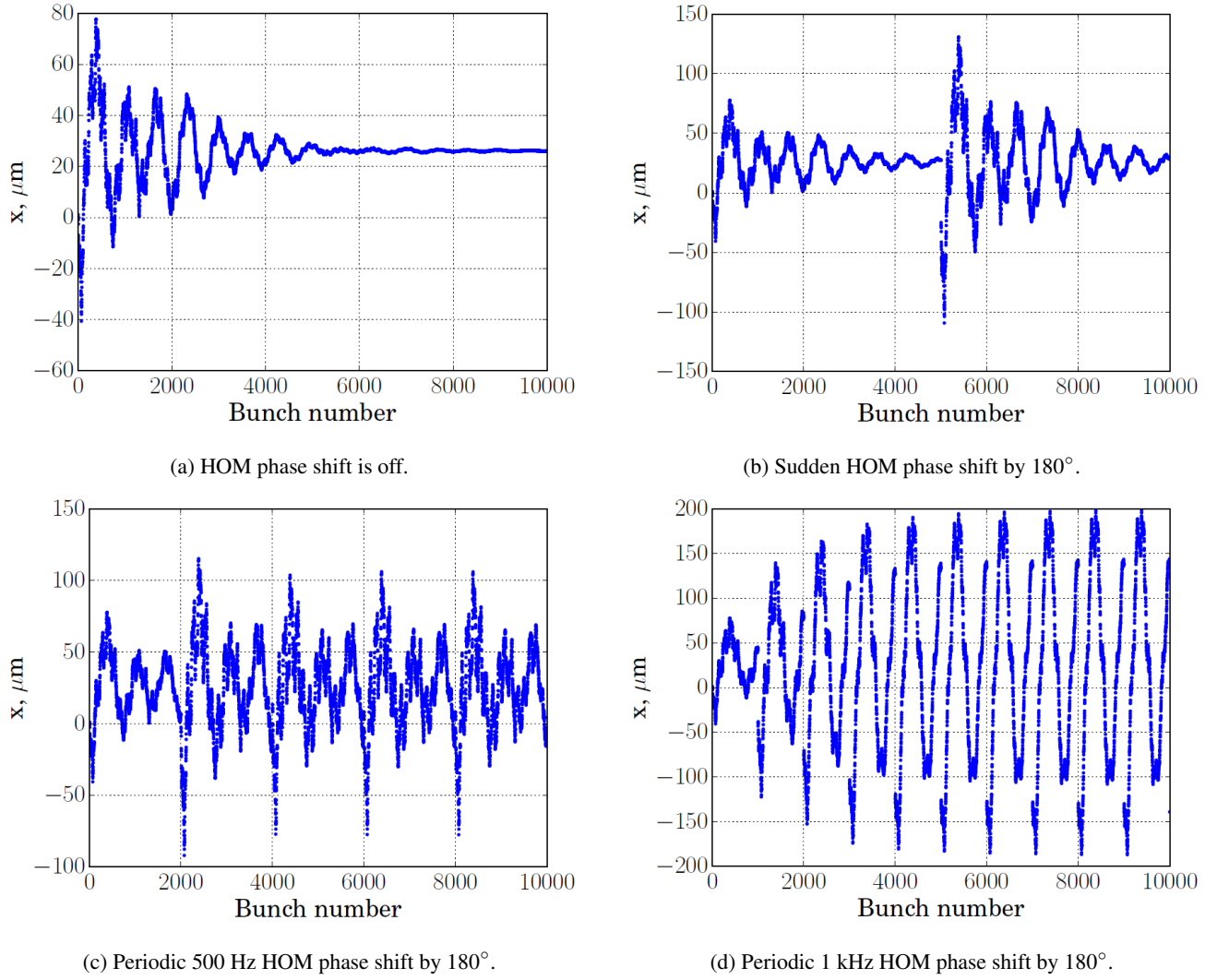

(d) Periodic 1 kHz HOM phase shift by 180°.

Figure 19: Transverse coordinate of electron bunches at the output of the linac.

to use additional HOM dumpers when existing HOM couplers reduce HOM quality factor down to $Q = 10^7$. The case of $Q = 10^7$ considered in the paper is extreme. HOM cause even less defects to the beam quality when quality factor is lower. Higher values of quality factor are not considered as $Q = 10^7$ is realistically achievable.

HOM transition effects for LCLS-II are analyzed. Major danger of the effect is coming from periodic changes in electron beam time structure. It is demonstrated that beam center position disturbance is below 200 μm for periodic 1 kHz HOM phase shift by 180 degree, which satisfies the LCLS-II beam dynamics requirements.

References

[1] LCLS II Conceptual Design Report

[2] **Need a reference for XFEL here**

[3] F. Marhauser, P. Hülsmann, H. Klein, *Trapped Modes in Tesla Cavities*, PAC 1999, New York, USA, 1999.

[4] A. Vostrikov, *et al., High order modes in 650 MHz sections of the Project X linac*, Fermilab TD Note 2011-008, 2011.

[5] A. Sukhanov, *et al., Resonance Excitation of Longitudinal High Order Modes in Project X Linac*, IPAC 2012, New Orleans, Louisiana, USA, May 20–25, 2012.

[6] H. Padamsee, J. Knobloch, and T. Hays, *RF Superconductivity for Accelerators*.

[7] Reuter and Sondheimer, Proc. R. Soc. A195, 336 (1948)

[8] Podobedov, Phys. Rev. STAB, 12, 044401 (2009)

[9] A. Sukhanov, *et al., Coherent Effects of High Current Beam in Project-X Linac*, LINAC 2012, Tel-Aviv, ISrael, September 9–14, 2012.

[10] A. Sukhanov, *et al., High Order Modes in Project-X Linac*, HOMCS12, Daresbury, UK, June 25–27, 2012, NIMA (in press)
`http://www.sciencedirect.com/science/`
`article/pii/S0168900213010796`

[11] D. G. Myakishev, V. P. Yakovlev, *The New Possibilities of SuperLANS Code for Evaluation of Axisymmetric Cavities*, PAC 1995, Dallas, Texas, USA, May 1–5, 1995.

[12] At least two models of HOM frequency spread based on measurements of HOM frequencies in production cavities exist. One is from Cornell, $\sigma_f \approx 10.9 \times 10^{-4}(f_{\text{HOM}} - f_0)$. Another model is from SNS, $\sigma_f \approx (9.6\text{–}13.4) \times 10^{-4}(f_{\text{HOM}} - f_0)$. We collect data on HOM frequency spread in Tesla cavities at Fermilab and will build our own model soon.

[13] P. Hülsmann *et. al*, *The Influence of Wakefields on Superconducting Tesla Cavities in FEL-operation*, Workshop on RF Superconductivity, Abano Terme, Italy, 1997.